HHS Public Access

Author manuscript

Biochemistry. Author manuscript; available in PMC 2023 March 01.

Published in final edited form as:

Biochemistry. 2022 March 01; 61(5): 385–397. doi:10.1021/acs.biochem.1c00696.

Anionic lipids confine cyt. c_2 to the surface of bioenergetic membranes without compromising its interaction with redox partners

Chun Kit Chan[‡,§], **Abhishek Singharoy**[‖], **Emad Tajkhorshid**[‡,⊥]

[‡]Theoretical and Computational Biophysics Group, NIH Center for Macromolecular Modeling and Bioinformatics, Beckman Institute for Advanced Science and Technology

[§]Department of Physics, University of Illinois at Urbana-Champaign, Urbana, IL 61801, USA

[‖]School of Molecular Sciences, Arizona State University, Tempe, AZ 85287, USA

[⊥]Department of Biochemistry, and Center for Biophysics and Quantitative Biology, University of Illinois at Urbana-Champaign, Urbana, IL 61801, USA

Abstract

Cytochrome c_2 (cyt. c_2) is a major element in electron transfer between redox proteins in bioenergetic membranes. While the interaction between cyt. c_2 and anionic lipids abundant in bioenergetic membranes has been reported, their effect on the shuttling activity of cyt. c_2 remains elusive. Here, the effect of anionic lipids on interaction and binding of cyt. c_2 to cytochrome bc_1 complex (bc_1) is investigated using a combination of molecular dynamics (MD) and Brownian dynamics (BD) simulations. MD is used to generate thermally accessible conformations of cyt. c_2 and membrane-embedded bc_1, which were subsequently used in multi-replica BD simulations of cyt. c_2 diffusion from solution to bc_1, in the presence of various lipids. We show that, counterintuitively, anionic lipids facilitate association of cyt. c_2 to bc_1 by localizing its diffusion to the membrane surface. The observed lipid-mediated bc_1-association is further enhanced by the oxidized state of cyt. c_2 in line with its physiological function. This lipid-mediated enhancement is salinity-dependent, and anionic lipids can disrupt cyt. c_2 - bc_1 interaction at non-physiological levels of salt. Our data highlight the importance of the redox state of cyt. c_2, the lipid composition of the chromatophore membrane, and the salinity of the chromatophore in regulating the efficiency of the electron shuttling process mediated by cyt. c_2. The conclusions can be extrapolated to mitochondrial systems and processes, or any bioenergetic membrane, given the structural similarity between cyt. c_2 and bc_1 and their mitochondrial counterparts.

Graphical Abstract

emad@illinois.edu .

Supporting Information. Detailed description of the methodology and Figures S1–S17.

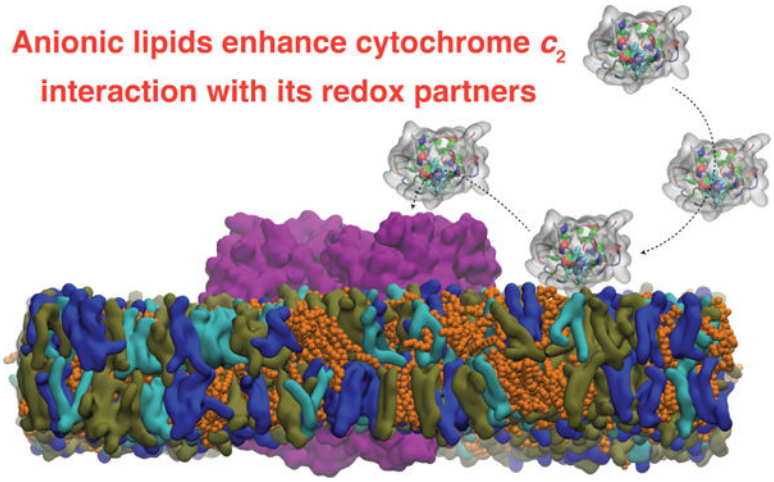

1 Introduction

The phototrophic purple bacterium is a photosynthetic microorganism commonly found in aquatic habitats.[1] It uses a cytoplasmic membrane vesicle rich in proteins, termed the chromatophore, to perform photosynthesis, thereby converting solar energy into chemical form that can be used by the cell.[2,3] As summarized in Fig. 1, major components of the chromatophore are the light harvesting LH1 and LH2 proteins, where the solar energy is absorbed. This energy migrates to the reaction center (RC) via excitation transfer, where it is used for charge separation via electron transfer processes.[4,5] The outcome is the reduced form of the cofactor quinone (quinol) that leaves the RC and diffuses to the cytochrome bc_1 complex (bc_1), where a proton-motive force is generated for biosynthesis of ATP.[6–9] Abstraction of an electron from bc_1 by the shuttle protein cytochrome c_2 (cyt. c_2), and docking of the reduced cyt. c_2 to the RC fills the electron hole and resets the system for another round of charge separation.[5,10]

Kinetic studies on the photosynthetic process of the chromatophore suggests a turnover time on the order of 25ms for electron transport mediated by quinol and cyt. c_2.[3,11,12] Within this time, rate measurements[3,8,11] infer that cyt. c_2 spends around 11.5ms close to bc_1, including the time for association and dissociation of the two proteins; whereas, only ~1.25ms is spent by cyt. c_2 at the RC site. The remaining 12ms, which is close to 50% of the total turnover time (25ms), is used by cyt. c_2 to diffuse between bc_1 and RC. The diffusion of cyt. c_2 is thus a substantial component of the electron-shuttling process mediated by the protein (Fig. 2).

The distributions of bc_1 and RC in the chromatophore are not even.[2,3,13,14] Using the chromatophore models (Fig. 1) constructed by our group[2,3] based on data from atomic force microscopy and negative stain electron microscopy, bc_1 homodimers are typically located in an expanded lipid buffer apart from the reaction center (RC); the typical nearest-neighbor distance between a bc_1 and an LH1-RC dimeric complex is approximately 5–10nm. However, many LH-RC dimers do not have nearby bc_1 complexes, thereby requiring cyt. c_2 diffusion distances to the nearest bc_1 of up to 20–30nm.

Cyt. c_2 possesses an intrinsic electric dipole moment, due to the protein's diametrically opposed positive and negative sides.[16,17] This property is believed to enable the protein to more efficiently associate with electronegative faces of its redox partners or with other charged macromolecules. Because of this property, the diffusion of cyt. c_2 can be sensitive to the electrostatic features of the chromatophore, most prominently the extensive presence of anionic lipids,[2,13,18,19] which are consistently present in all bioenergetic membranes, as well as fluctuations in the chromatophore's salinity.[14,20] As a matter of fact, in our earlier simulations of the chromatophore membrane, using phosphatidylglycerol (PG) to represent anionic lipids, we observed frequent binding of cyt. c_2 to lipids at low salinity, resulting in an inaccurate calculation of binding behavior of cyt. c_2 to bc_1.[14]

Interaction with anionic lipids can also have other potential effects on the structural stability of the protein. Studies on cytochrome *c*, the counterpart of cyt. c_2 in mitochondria (Fig. S1), have reported deformation of the protein upon its interaction with cardiolipin (CL),[21,22] a major anionic lipid found in the chromaotophore and mitochondrial membranes.[2,13,18,19]

The solvent-exposed surfaces of bc_1 (Fig. S2) and RC,[17] the two redox partners of cyt. c_2, are negative on the periplasmic side. Upon association, cyt. c_2 uses its positive side to dock to the surface of its redox partners, followed by additional stabilization through hydrophobic interactions,[8,16,17,23] a process also reported for the homolog protein, cytochrome *c*.[24,25] For this reason, anionic lipids, which increase the negative charge density of the membrane surface, can potentially present an undesirable competition, distracting cyt. c_2 from its redox partners. Notably, anionic lipids such as PG and CL have their own functional roles in the chromatophore, e.g., facilitating proton translocation and maintaining structural stability of transmembrane proteins.[26–29] Nevertheless, their negative charges can in principle interfere with the shuttling activity of cyt. c_2.

In this study, the impact of anionic lipids on diffusive behavior of cyt. c_2, and its encounter and association with bc_1 are investigated using a combination of molecular dynamics (MD) and Brownian dynamics (BD) simulations. MD was used to generate thermally accessible conformations of cyt. c_2 and membrane-embedded bc_1, followed by multi-replica BD simulations of cyt. c_2 diffusion on the surface of membranes with and without anionic lipids, at varying salinity levels, and with all possible combinations of oxidized and reduced cyt. c_2 and bc_1. Both PG and CL were included in the membranes studied here to provide a more realistic representation of the membrane and its charge. Earlier studies on soluble protein elements of bioenergetic systems,[30] such as cytochrome *c*,[31] cyt. c_2,[14] cytochrome c_6,[32] and plastocyanin,[32,33] have demonstrated BD simulations as an effective approach to characterize protein diffusion and complex formation in an environment-dependent manner.

Our results show that anionic lipids confine diffusion of cyt. c_2 to the surface of the membrane. Interestingly, and despite what might be assumed intuitively about the competition between anionic lipids and bc_1, surface-confined diffusion of cyt. c_2 promotes its association to bc_1, and, as importantly, it does not seem to interfere the redox-dependence of their association, allowing the two partners with complementary redox states to bind more frequently. These properties allow anion-rich bioenergetic membranes to provide a favorable environment for the electron-shuttling role of cyt. c_2. Lastly, we show that the role of anionic

lipids in mediating more effective cyt. c_2 - bc_1 association is tunable by the salinity of the system. Variations in salinity can modulate the electrostatic interactions between cyt. c_2 and both anionic lipids and bc_1, likely to different extents given the heterogeneity in the distribution of charges in these species. Such a tunable role of anionic lipids may be of importance in regulating electron-shuttling efficiency of the chromatohpore and other bioenergetic systems under different living conditions of the cell.

2 Methods

In this part, the procedures to set up, execute, and analyze the simulations are outlined (Fig. S3). First, in Sec. 2.1, MD simulations necessary to generate *in-vivo*-like conformations for different redox forms of cyt. c_2 and membrane-embedded bc_1 are described. Then, in Sec. 2.2, we explain rigid-body modeling of cyt. c_2 based on structural information from MD simulations. Next, in Secs. 2.3 and 2.4, the construction of mean-field representations that describe long-range (electrostatic) and short-range (van der Waals (vdW)) forces from membrane-embedded bc_1 acting on cyt. c_2 is discussed. Lastly, in Sec. 2.5, a brief description is provided on how the cyt. c_2 model together with the mean-field representations for membrane-embedded bc_1 are used in BD simulations. Protocols for various analyses on the resulting BD trajectories are described in Secs. S1.3, S1.4, and S1.5.

2.1 Modeling and MD simulations of cyt. c_2 and membrane-embedded bc_1

The initial structure for bc_1 was adopted from the PDB: 2QJY.[35] By assigning proper redox states to the heme prosthetic groups associated with the protein (Fig. S4(B)), suitable models for MD simulations of the redox forms of bc_1 were constructed, namely the oxidized bc_1 ($C1_{ox}$) and the reduced bc_1 ($C1_{red}$). Model preparation was performed using the AUTOPSF plugin of VMD[36] with the CHARMM36m force field[37] and parameters obtained by earlier quantum chemical calculations.[38] The protonation states of protein residues were set to their default states at pH 7.

Each redox form of bc_1 was uploaded to the Orientations of Proteins in Membranes (OPM) database[39] to determine the protein alignment in a lipid bilayer. Each aligned redox form was then embedded in a lipid bilayer using the MEMBRANE BUILDER tool of CHARMM-GUI.[40–43] In this study, two types of lipid bilayers were employed. The first was a control bilayer only consisting of phosphatidylcholine (PC) phospholipids. The second adopted a lipid composition similar to that of the chromatophore membrane and consisted of 19% PC, 17% phosphatidylethanolamine (PE), 35% phosphatidylglycerol (PG), and 29% cardiolipin (CL).[13] Both PG and CL carry negative charges. This anionic bilayer is referred here as the chromatophore-like (ChP) bilayer. In total, four membrane-embedded bc_1 were constructed for MD simulations, namely (1) $C1_{ox}$ with a ChP bilayer, (2) $C1_{red}$ with a ChP bilayer, (3) $C1_{ox}$ with a control (PC) bilayer, and (4) $C1_{red}$ with a control bilayer.

Determining the pKa for CL at physiological pH and within a membrane environment has been an active area of research.[44–47] The protonation state of CL lipids can be dynamically coupled to other charged lipids and proteins within the membrane, and even affected by the movement and conformational changes of the CL molecules within their local environment of the membrane. Recent data point to an even lower pKa for some CL lipids, and thus

an overall charge of −2,[46,47] compared to earlier studies suggesting an overall charge of −1.[44,45] Since the net charge of CL cannot change during our classical simulations, we opted an overall charge of −1 for CL.

Models of cyt. c_2 for MD simulations were constructed in a manner similar to bc_1. The initial structure for the reduced cyt. c_2 ($C2_{red}$) was adopted from PDB: 1L9B,[48] which featured a complex of $C2_{red}$ with RC. The initial structure for the oxidized cyt. c_2 ($C2_{ox}$) was adopted from a previous MD simulation,[8] which featured a stable complex of $C2_{ox}$ with bc_1. These two structures were converted into models ready for MD simulations using AUTOPSF plugin of VMD[36] and with the same parameter set employed for bc_1. The resulting $C2_{red}$ is with a net charge of −2 while $C2_{ox}$ is with a net charge of −1. The oxidation state of the heme group of cyt. c_2 follows the redox state of the protein.

All redox forms of membrane-embedded bc_1 and cyt. c_2 were solvated and ionized at 0.15M salinity using VMD.[36] The solvated and ionized system for each redox form of cyt. c_2 was simulated for 150ns using NAMD 2.13.[49,50] Both redox forms reached equilibrium after 100ns exhibiting stable fluctuations in root mean squared deviation (RMSD) of the protein backbones and their electric dipole moment (Fig. S5). The last snapshot of each trajectory was employed as the model of cyt. c_2 for the BD simulations (Sec. 2.2). Each solvated and ionized membrane-embedded bc_1 was simulated for 300ns to reach equilibrium. For each membrane type, extending from the last snapshot of the corresponding trajectory, 5 independent 5ns-long MD simulations were performed. These trajectories sampled the structural fluctuation of the membrane. Their use are discussed in Sec. 2.3, Sec. 2.4. The explicit protocols for equilibrating membrane-embedded bc_1 and cyt. c_2 are described in Sec. S1.1.

2.2 Deriving parameters for BD simulations of cyt. c_2

After being equilibrated, each redox form of cyt. c_2, represented by the last snapshot of the corresponding MD trajectory (Sec. 2.1), was modelled as a rigid body for the BD simulations of its diffusion on the surface of the membrane. This rigid-body model, as a coarse-grained representation, used a set of parameters and grids to describe the response of cyt. c_2 to hydrodynamics, electrostatics, and vdW forces. The parameters and grids, and the approach used to determine them are explained below in Sec. 2.2.1, Sec. 2.2.2, and Sec. 2.2.3. On the other hand, potentials that served as mean-field representations for the environment that cyt. c_2 diffuses in are discussed in Sec. 2.3 and Sec. 2.4.

2.2.1 Frictional coefficients of cyt. c_2—The hydrodynamic response of cyt. c_2 was described by setting coefficients for translational and rotational frictions. For each redox form of cyt. c_2, its principal axes were first determined in VMD.[36] The protein was then orientated to let the top three principal axes align with the x, y, and z axes, respectively. This orientation gave a diagonalized moment of inertia tensor for the protein. A pdb file of the protein with this orientation was then fed into the program, Hydropro,[51] to estimate its diffusion tensor. The diagonal components of this diffusion tensor were then converted to translational friction coefficients and rotational friction coefficients using Stokes-Einstein

relation,[14,51] together with the mass of the protein and its pre-determined moment of inertia tensor.

2.2.2 Charge distribution of cyt. c_2—The electrostatic response of cyt. c_2 to any electrostatic potential is described through its charge distribution. For each redox form of cyt. c_2, a continuum representation of its charge distribution was computed using its partial atomic charges with the VOLMAP plugin of VMD.[36] These representations were stored by VMD[36] as grids, which were 3-dimensional volumetric maps that contained a value at each grid point. During BD simulations, these grids were utilized with electrostatic potentials derived from different bc_1-embedding membranes to determine electrostatic forces on cyt. c_2. The determination of electrostatic potentials for bc_1-embedding membranes and the corresponding forces on cyt. c_2 are discussed in Sec. 2.3.

2.2.3 Representation of vdW forces on cyt. c_2—The vdW forces acting on cyt. c_2 were constructed from its environment using the CHARMM force field description of the vdW interaction energy between atom pairs, i and j:

$$U_{ij}^{LJ} = \epsilon_{ij}\left[\left(\frac{r_{ij}^{min}}{r_{ij}}\right)^{12} - 2\left(\frac{r_{ij}^{min}}{r_{ij}}\right)^{6}\right], \tag{1}$$

where r_{ij} is the distance between atoms i and j, $r_{ij}^{min} = \frac{1}{2}\left(r_i^{min} + r_j^{min}\right)$, and $\epsilon_{ij} = \sqrt{\epsilon_i \epsilon_j}$. The Lennard-Jones (LJ) parameters for atom i were r_i^{min} and ϵ_i; and those for atom j were r_j^{min} and ϵ_j. The vdW force on atom i from atom j was derived from Eq. 1 as

$$\vec{F}_{i \leftarrow j} = -\vec{\nabla}_i U_{ij}^{LJ}. \tag{2}$$

Using Eq. 2, a coarse-grained representation that describes the response of cyt. c_2 to vdW forces form its environment was developed. First, K-mean clustering[52,53] was applied to the LJ parameters of every atom of cyt. c_2. Atoms with their LJ parameters belonging the same cluster were then classified into the same atom group. The 4 resulting atom groups were: (1) heavy atoms for the pyrrolidine of each proline; (2) all other heavy atoms except sulphur atoms; (3) sulphur atoms; and (4) hydrogen atoms. Each atom group denoted a representative atom type with the centroid $\left(\left(r_{centroid}^{min}, \epsilon_{centroid}\right)\right)$ of the corresponding cluster being its LJ parameters (Sec. S1.2). Then, a continuum representation of the particle distribution for each atom group was computed by the VOLMAP plugin of VMD.[36] These representations were stored as grids. During BD simulations, these grids were utilized with the potential of mean force (PMF) derived from different bc_1-embedding membranes to determine vdW forces acting on cyt. c_2 using Eq. 2. The determination of PMF for bc_1-embedding membranes is discussed in Sec. 2.4.

2.3 Electrostatic potentials of bc_1-embedding membranes

For each redox form of cyt. c_2, its charge distribution (ρ_{C2}) and the electrostatic potential of the environment (V_{EN}) determined the translational electrostatic force on it during the BD simulations as

$$\vec{F}_{C2}^{tran}\left(\vec{r}\right) = \int_{C2} d\vec{\eta}\left\{\rho_{C2}\left(\vec{r}+\vec{\eta}\right)\left[-\vec{\nabla}V_{EN}\left(\vec{r}+\vec{\eta}\right)\right]\right\}, \tag{3}$$

where $\vec{r}$ is the center of mass (COM) of cyt. c_2. This integration was performed over the entire protein, as denoted by $\int_{C2}$. Similarly, the torque on cyt. c_2 about any of its principle axes, $\vec{l}$, which passes through $\vec{r}$, was given by

$$T_{C2}^{rot}\left(\vec{r},\vec{l}\right) = \int_{C2} d\vec{\eta}\left\{\vec{\eta} \times \left[-\rho_{C2}\left(\vec{r}+\vec{\eta}\right)\vec{\nabla}V_{EN}\left(\vec{r}+\vec{\eta}\right)\right]\right\}\cdot\vec{l}\,. \tag{4}$$

Charge distribution of cyt. c_2 was determined as outlined in Sec. 2.2.2.

The electrostatic potential, V_{EN}, was determined for each bc_1-embedding membrane, as the environment that cyt. c_2 interacted with during BD simulations. To determine V_{EN}, multiple MD trajectories for each bc_1-embedding membrane (Sec. 2.1) were employed. First, along each trajectory, snapshots describing the partial charge distribution for the membrane were selected at 1-ns intervals. These snapshots were aligned with the COM of bc_1 located at the origin. Then, the partial charge distribution for each of these snapshots was input to the program, Adaptive Poisson-Boltzmann Solver (APBS),[54,55] to determine the corresponding electrostatic potential at the temperature 300K. Electrostatic screening effects from water molecules and ions were modeled in APBS by specifying different salt concentrations: 0.02M, 0.15M, and 0.40M. Lastly, these potentials were averaged to produce the electrostatic potential for the corresponding bc_1-embedding membrane at the specified salinity. This electrostatic potential was then used to produce the corresponding electrostatic forces acting on cyt. c_2.

2.4 Mean-field representation for vdW forces acting on cyt. c_2 from bc_1embedding membranes

The vdW forces acting on cyt. c_2 from a bc_1-embedding membrane was determined through the potential of mean force (PMF) of the later one. For each bc_1-embedding membrane, the corresponding set of MD trajectories (Sec. 2.1) were used to compute its PMF through a free energy perturbation technique, Implicit Ligand Sampling (ILS),[56] based on the representative atom types described in Sec. 2.2.3. First, each of the MD trajectories was aligned with the COM of bc_1 located at the origin. Then, using VMD,[36] ILS calculations were performed on each of trajectory at 1-ns intervals and at a temperature of 300K with the use of each representative atom type as a probing point particle. Each ILS calculation determined a 3-dimensional PMF for the corresponding trajectory based on vdW interaction

energy between the probing particle, characterized by $r^{min}_{centroid}$ and $\epsilon_{centroid}$ (Sec. 2.2.3), and the bc_1-embedding membrane. Lastly, the 3D PMF calculated for individual trajectories were averaged and assigned to the corresponding bc_1-embedding membrane as its PMF for the respective representative atom types.

The PMF for each representative atom type was utilized to determine the vdW forces on a cyt. c_2. For atoms corresponding to each representative atom type in cyt. c_2, the vdW forces were given by Eq. 3 and Eq. 4; with the charge distribution in the equations replaced by the particle distribution of these atoms and with the electrostatic potential replaced by the corresponding PMF. The vdW forces on atoms of each representative atom type were then summed up to give the total vdW forces on cyt. c_2. The same protocol was used for the torques on cyt. c_2 that arose from vdW forces.

2.5 Setup of BD simulations of cyt. c_2

BD simulations were performed at salt concentrations of 0.02M, 0.15M, and 0.40M using the code, Atomic Resolution Brownian Dynamics (ARBD).[14,57] In ARBD, each diffusing cyt. c_2 was represented as an atomistic rigid body, with its particle and charge distributions characterized by pre-computed grids (Sec. 2.2). Each bc_1-embedding membrane, represented by its PMF (Sec. 2.4) and its electrostatic potential at the specific salinity (Sec. 2.3), mimicked a static environment that interacted with cyt. c_2. During the BD simulations, ARBD summed up the interaction energy between individual grids and the corresponding potentials and derived forces and torques on cyt. c_2 from the total interaction energy. These forces, together with coefficients of friction (Sec. 2.2.1), described the Brownian dynamics of cyt. c_2 in the presence of a bc_1-embedding membrane.

For each level of salinity, four sets of BD simulations, denoted as $C1_{ox}C2_{red}$-ChP, $C1_{red}C2_{ox}$-ChP, $C1_{ox}C2_{red}$-PC, and $C1_{red}C2_{ox}$-PC, were performed. The indices X and Y in "$C1_XC2_Y$" are used to describe the redox states of the partners, bc_1 (X) and cyt. c_2 (Y), with the abbreviations "ox" and "red", referring to the oxidized and reduced states, respectively. The suffixes, "-ChP" and "-PC", indicate the lipid bilayer employed for the simulations, with the former representing a chromatophore-like bilayer (Sec. 2.1) and the latter a control (PC only) bilayer. Each set of BD simulations consisted of 400 replicas of a 1μs-long simulations. These simulations were run in parallel on 20 gpus, with each gpu hosting 20 replicas. At the beginning of these simulations, copies of cyt. c_2 were placed randomly on the periplasmic side of the bc_1-embedding membrane, with the COM of each cyt. c_2 set above the maximum height of the cyt. c_2-bc_1 binding interface by 50 Å (Fig. S6). Simulations with the two different bilayers are here termed as ChP and PC simulations, respectively. Collectively, the BD simulations have accumulated (4×400×0.001 =) 1.6ms sampling of cyt. c_2 diffusion in the presence of a membrane.

It is worth mentioning that a living organism is very unlikely to undergo such a wide variation in their intracellular salt concentration, from 0.02M to 0.40M. The conditions that we used are to replicate *in vitro* experiments reported,[58] to theoretically test the response of the system to extreme salt concentrations. Also, the effective ion concentration in a cellular environment depends on its level of protein crowding.[59] A recent study has shown

that the effective ion concentration for *Escherichia coli* (*E. coli*) can be as low as 0.02M despite the system having a concentration of 0.15M for cations. In our current set of simulations, we do not have a representation for cellular crowding that may complicate the electrostatic effects. Each cyt. c_2 was simulated individually, with a net charge of only −1 to −2, depending on the protein's redox state. Thus, the electronegativity presented in the bulk in our simulations is substantially less than that in *E. coli*, which includes a large copy number of electronegative macromolecules.[59] However, under such conditions, effective ion concentration are expected to likely drop, weakening ionic screening of electrostatic forces. Under such condition, attraction between cyt. c_2 and bc_1 as well as lipids will increase.

3 Results and Discussion

In what follows, first, we demonstrate that anionic lipids confine the diffusion of cyt. c_2 to the surface of the membrane. Then, we show that this confined diffusion is beneficial to the association of cyt. c_2 and bc_1. We also illustrate that the likelihood and lifetime of cyt. c_2-bc_1 association can change with the redox states of the two proteins. Finally, we describe how varying the salt concentration modulates the interaction of cyt. c_2 with both the anionic lipids and with bc_1.

3.1 Anionic lipids confine diffusion of cyt. c_2 to the surface of membrane.

Cyt. c_2 has an intrinsic electric dipole,[16,17] which helps aligning it with the negatively charged surface of bc_1 on the periplasmic side of the chromatophore.[8] At the same time, this dipole can also mediate association of cyt. c_2 with the chromatophore membrane, which is overall negatively charged due to abundant anionic lipids.[13,14]

Compared with the control simulations employing a POPC bilayer, cyt. c_2 - lipid associations with the chromatophore-like (ChP) bilayer (Sec. 2.1 of Methods) was found to be 2–8 times more frequent (2 and 8 folds for the reduced ($C2_{red}$) and oxidized cyt. c_2 ($C2_{ox}$), respectively) (Fig. S7). As a consequence, the number of cyt. c_2 - bc_1 binding events mediated by cyt. c_2 - lipid association, referred to as Lipid-Mediated Association of cyt. c_2 to bc_1 ($LMA_{C2\rightarrow C1}$; Fig. 3A), turns out to be at least 20 times larger for the ChP bilayer compared to control (Fig. S8). Among the 400 cyt. c_2 simulations with the ChP bilayer, ~100 display instances of $LMA_{C2\rightarrow C1}$, sometimes multiple times (Fig. S9). In contrast, in control simulations, only less than 10 cyt. c_2 display $LMA_{C2\rightarrow C1}$. These results suggest that the presence of anionic lipids facilitate the binding of the two redox partners, and that $LMA_{C2\rightarrow C1}$ seem to constitute a major mechanism for cyt. c_2 association with bc_1 in the chromatophore.

Upon binding to anionic lipids, cyt. c_2 continues its effective diffusion on the surface of the membrane, a necessary condition for binding to bc_1, even though one might expect binding to lipids to limit its lateral motion (Fig. 3B). While diffusing, cyt. c_2 spends around 30 − 40% of its time, on average, in the vicinity of the lipid bilayer (Fig. 3C). Even when cyt. c_2 diffuses in the bulk solution, it maintains a closer distance to the lipid bilayer (Figs. 3C and S10)). Therefore, it can be concluded that anionic lipids, by confining diffusion of cyt. c_2 closer to the membrane surface, promote its binding and interaction with the redox partner. A representative trajectory for this confined diffusion is shown in (Fig. 3D).

For cyt. c_2 copies engaged in $LMA_{C2\rightarrow C1}$, the distance between their first membrane encounter point and bc_1 follows a Gaussian-like distribution (Fig. S11). This distribution has a mean value around 110 Å, and a standard deviation of ~ 20 Å. A membrane-associated cyt. c_2 positioned this far from bc_1 (Fig. 3E), is unlikely to feel any electrostatic forces (attraction) from bc_1. However, because of the membrane-mediated confined diffusion, the likelihood for cyt. c_2 to be in the vicinity of the lipid bilayer is higher, which in turn results in a higher likelihood to locate and associate with bc_1. This mechanism, mediated by the the anionic lipids potentially applies to any transmembrane redox partner of cyt. c_2. For example, the cyt. c_2 - RC association can be expected to also be improved in the presence of anionic lipids.

During our simulations, regardless of its redox state, cyt. c_2 associates more likely with PG than CL (Fig. S12). This phenomenon might be attributed to the higher head-group charge density in PG, when compared with CL. As a result, PG is more recognizable by the basic residues in cyt. c_2 as it approaches the lipid bilayer. In our current study, no stable complex between cyt. c_2 and PG or CL was observed. Cyt. c_2-lipid associations that led to cyt. c_2-bc_1 associations were dominantly transient (Fig. 3B). However, complex formation with either PG and CL can trigger peroxidase activity in cytochrome *c*,[60] a homolog of cyt. c_2. This activation, which is attributed to modulations of cytochrome *c* dynamics without major denaturation, was found to be more pronounced upon CL binding. Thus, potential adverse effects for complex formation with either PG or CL remain a concern for cyt. c_2. However, CL has been reported to have clear binding pockets in the vicinity of integral membrane proteins, including those involved in electron-transfer reactions.[61–63] In contrast, PG lipids are more free to diffuse in bioenergetic membranes and less likely to have specific interactions with proteins. The reported differential behavior of PG and CL, along with our simulation results (Fig. S12), suggest electron-shuttling proteins like cytochrome *c* may be more likely to encounter PG than CL *in vivo*.

3.2 Redox dependence of the association between cyt. c_2 and bc_1

The impact of the redox states on the likelihood of cyt. c_2 - bc_1 association was probed in two sets of BD simulations. In the first, reduced cyt. c_2 ($C2_{red}$) was simulated in the presence of oxidized bc_1 ($C1_{ox}$); in the second, oxidized cyt. c_2 ($C2_{ox}$) was simulated with a reduced bc_1 ($C1_{red}$). For each set, simulations were repeated either with the ChP bilayer or with the control bilayer (pure POPC).

Regardless of the lipid bilayer used, BD simulations showed consistently higher cyt. c_2 association with bc_1 for $C2_{ox}$ than $C2_{red}$ (Fig. 4A). Thus, the association likelihood between cyt. c_2 and bc_1 seems to be dependent on the redox states of the two proteins. This result favors the physiological direction of electron transfer between the redox partners; $C2_{ox}$ association with $C1_{red}$ is needed for electron uptake while $C2_{red}$ needs to depart from $C1_{ox}$ for the next round of electron shuttling. We note that in our models the surface area of lipids is ~ 5 times of that of bc_1 (Fig. S2A), providing abundant opportunities for lipids to compete with bc_1 for cyt. c_2 binding. With this in mind, the observed redox dependence appears to represent a robust feature.

Regardless of the redox states of the two proteins, cyt. c_2 association with bc_1 is slightly higher with the ChP bilayer than the control membrane (Fig. 4A). This observation is consistent with our speculations in Sec. 3.1. To further examine the role of $LMA_{C2\rightarrow C1}$ in this enhancement, cyt. c_2 trajectories were divided into two groups. In the first group, cyt. c_2 associated with bc_1 without any prior encounter with lipids. This mechanism is termed here as Direct Association of cyt. c_2 to bc_1 ($DA_{C2\rightarrow C1}$). On the other hand, cyt. c_2 in the second group associated bc_1 through $LMA_{C2\rightarrow C1}$. Our grouping of cyt. c_2 trajectories for the case of $C1_{red}$ and $C2_{ox}$ shows that the enhancement to cyt. c_2 - bc_1 association from $LMA_{C2\rightarrow C1}$ is not necessary straightforward. For the case of $C1_{red}$ and $C2_{ox}$, the fraction of cyt. c_2 associated with bc_1 through $DA_{C2\rightarrow C1}$ is similar to that recorded with the control membrane at the early half of the simulation ($t < 500$ns). However, at the later half of the simulation ($t \geq 500$ns), this fraction drops and becomes appreciably below that with the control membrane by the end of our simulations (Fig. 4B). One possible explanation for this drop is that $C2_{ox}$ may have a high association affinity with lipids, and thus some $C1_{red}$ - associated $C2_{ox}$ are lost to lipids as the time passes. However, this affinity also facilitates $C2_{ox}$ association with lipids, then with $C1_{red}$ through $LMA_{C2\rightarrow C1}$. In fact, our simulations show that the above-mentioned drop is made up by cyt. c_2 - bc_1 associations from $LMA_{C2\rightarrow C1}$, allowing the fraction of cyt. c_2 associated with bc_1 with the ChP bilayer to be overall higher than that with the control membrane. This observation shows that the role of $LMA_{C2\rightarrow C1}$ in enhancing cyt. c_2 - bc_1 associations can be sensitive to the affinity of cyt. c_2 to lipids, which, while allowing the presence of $LMA_{C2\rightarrow C1}$, can also compete against bc_1 in recruiting cyt. c_2. This sensitivity suggests that the actual role of anionic lipids in the chromatophore, rather they are facilitating or interrupting cyt. c_2 shuttling of elections, can be quite dependent on the condition of the vesicle, such as local variations of lipid compositions.

Lastly, the distributions for the minimum heme-to-heme distance between the heme group of cyt. c_2 (oxidized) and the reduced heme of reduced bc_1 were computed (Fig. S13). Due to the rigid representations used in the BD simulations, the eventual heme-heme distance after each encounter, which would depend on conformational relaxations of the two proteins,[8] is not sampled here. Yet, our computed distributions show that, compared with PC simulations, ChP simulations offer slightly closer cyt. c_2 association to bc_1 with heme-to-heme separations within physiologically observed values (8.4Å to around 9.4Å).[8,24,48]

3.3 Redox states of cyt. c_2 modulate residence on electronegative association partners.

In Sec. 3.2, we see that the redox states of cyt. c_2 and bc_1 modulate the affinity of the two proteins, even under an abundant presence of anionic lipids. To examine how this modulation may arise, especially for cyt. c_2, which also associate with lipids, we quantify the association of cyt. c_2 to its association partner, namely bc_1 or lipids, by a 2-parameter model (Sec. S1.4). The first parameter, coined the recognition probability, is the likelihood for cyt. c_2 to recognize and associate to an association partner when approaching it. The second parameter, coined the residence probability, is the likelihood for cyt. c_2 to remain associated with a partner after binding to it. These probabilities were then determined by fitting[64] our 2-parameter model to the respective distributions of residence time between each redox form of cyt. c_2 and each of its association partners. Our results (Table 1) show

that $C2_{ox}$ has only a marginally higher recognition probability than $C2_{red}$, regardless of whether the association partner is bc_1 or lipids. On the other hand, the residence probability of $C2_{ox}$ is noticeably higher than that of $C2_{red}$, ranging from 0.07 (20% higher) to 0.09 (26% higher), depending on whether the association partner is bc_1 or lipids. Thus, the different redox states of cyt. c_2 predominantly affect the likelihood for cyt. c_2 to stay with its association partners after associations.

To explore how the redox state of cyt. c_2 affects the protein residence on its association partners, we examine the probability for individual residues of cyt. c_2 to make contacts with association partners after cyt. c_2 associated with them. These probabilities, coine as association probabilities, were determined for each redox form of cyt. c_2 (Fig. 5A). Residues with non-zero association probabilities are generally conserved between the two redox forms. The individual probabilities are, however, largely redox-dependent. To illustrate this dependence, residues with probabilities >0.25 were identified for each redox form, i.e, the residues that make contacts with binding partners over 1/4 of the time of the association. These residues serve as representative hotspots for which the protein associations with bc_1 or lipids occur (termed hotspot residues and are visualized in Fig. 5B). The hotspot residues for $C2_{red}$ are almost all basic (R32, K35, K55, K88, K97), but also include one polar (T101) and one non-polar (A34) residue. Those for $C2_{ox}$ are partitioned roughly equally to basic residues (K10, R32, K95, K97, K103, K105) and polar residues (N13, Q14, T17, N33, T101). The larger number of basic hotspot residues in $C2_{ox}$ indicates a stronger electrostatic attraction over $C2_{red}$ upon association with electronegative lipids or proteins. Also, the total number of hotspot residues for $C2_{ox}$ is around 1.5 times of that for $C2_{red}$ Fig. 5B). Thus, upon association, $C2_{ox}$ is more likely than $C2_{red}$ to have multiple residues simultaneously making contacts with an association partner, which, subsequently, allows $C2_{ox}$ to develop a stronger vdW attraction with its partner than $C2_{red}$. Our results here are in line with and substantiate $C2_{ox}$ higher residence probability with any association partner than $C2_{red}$. These results also suggest variations in the positions of residues at the electro-positive side of cyt. c_2, which can arise upon a change of redox state, can underlie the modulations on cyt. c_2 affinity with electro-negative association partners.

The overall conformation of cyt. c_2 is barely affected upon changes in its redox state (C_α RMSD = 1.4Å). However, some residues display noticeably higher displacement than the others (>4Å) (Fig. 5C), including K95, a hotspot residue in $C2_{ox}$. These residues are all located at the flexible outermost coil region of cyt. c_2. Their positional change likely affects the initial encounter of cyt. c_2 with its partners, and subsequently alter the likelihoods for other residues to come close to the association partners. Thus, subtle structural differences between $C2_{ox}$ and $C2_{red}$ in this flexible coil region may underlie the observed difference in the observed residence probabilities. It is worth noticing that the above observation, where changes in the redox state of cyt. c_2 can only give rise to structural variations in flexible regions, is in line with NMR experiments on cyt. *c*, a homologue of cyt. c_2, from human[65] and other species.[66–69]

3.4 Ionic strength modulates the impact of anionic lipids in cyt. c_2-bc_1 association.

Anionic lipids participate in the associations of cyt. c_2 with bc_1 by confining the diffusion of cyt. c_2 in a region close to the membrane (Sec. 3.1). The cyt. c_2 - lipid interaction is electrostatic in nature, and thus, should be susceptible to variations in the salinity, which often emerges when bioenergetic systems are under stress.[14,20] The impact of such a variation on the role of lipids in mediating cyt. c_2 - bc_1 association was probed by comparing BD simulations at 0.40M and 0.02M salinity, representing a high and a low salt environment for the chromatophore, respectively.[58]

At high (0.40M) salinity, the time evolution of the fraction of cyt. c_2 associated with bc_1 along BD simulations with the ChP bilayer is remarkably similar to that for the control (Fig. 6A). In particular, the fraction of $LMA_{C2\rightarrow C1}$ is practically negligible when compared to that at 0.15M salinity (Fig. 4B). Also, the fraction of cyt. c_2 associated with bc_1 for $C2_{ox}$ is hardly distinguishable from that of $C2_{red}$. These observations are in line with the strong screening of charges at high salinity, which diminishes substantially the electrostatic attraction between cyt. c_2 and anionic lipids, making the electrostatic attraction from the ChP bilayer much less effective at the long range (Fig. S14).

Also, upon weakened attraction, lipid-associated cyt. c_2 can dissociate from lipids more easily due to thermal fluctuations. Thus, the electrostatic attraction of the ChP bilayer towards cyt. c_2 has become a weak force only acting at short-ranges. In other words, the ChP bilayer acts like the electroneutral control bilayer. Similarly, differences between $C2_{ox}$ and $C2_{red}$ in terms of their attraction to bc_1 or lipids becomes negligible upon charge screening. In fact, the failure to differentiate $C2_{ox}$ from $C2_{red}$ impedes the ability of bc_1 to recruit $C2_{ox}$ and release $C2_{red}$ upon a change of the redox state, and subsequently reduces the likelihood for bc_1 to form productive association with cyt. c_2. A high salt environment is therefore undesirable for energy transduction in the chromatophore.

At low (0.02M) salinity, the fraction of cyt. c_2 associated with bc_1 in BD simulations with $C2_{ox}$ is noticeably higher than $C2_{red}$. This situation is in contrast to BD simulations at 0.40M salinity (Fig. 6(A)), and reflects the ability of bc_1 to differentiate $C2_{ox}$ from $C2_{red}$ at low salinity. However, the enhancement to cyt. c_2 - bc_1 association upon the presence of anionic lipids, which is present at 0.15M salinity, is absent. At 0.02M salinity, the fraction of cyt. c_2 associated with bc_1 in BD simulations with the ChP bilayer is either similar to (in the case of $C2_{red}$) or significantly lower than (in the case of $C2_{ox}$) the control (Fig. 6B). Thus, at low salinity, the presence of anionic lipids does not seem to facilitate cyt. c_2 - bc_1 association.

The presence of anionic lipids fails to improve cyt. c_2 - bc_1 association at low salinity when compared with the control. This phenomenon was further analyzed by visualizing the electrostatic potential of bc_1 at 0.15M and 0.02M salinity. As can be seen clearly, with low salinity, contour surfaces representing negative electrostatic potential can extend noticeably further (Fig. 6(C)). These expansions allow bc_1 to reach cyt. c_2 located at farther distances and subsequently attract it. For these cyt. c_2, associating to bc_1 through $LMA_{C2\rightarrow C1}$ appears to be unnecessary. A reduced salinity also strengthens the attraction between cyt. c_2 and anionic lipids, likely lengthening the time that cyt. c_2 resides on the ChP bilayer. In fact, the

fraction of $C2_{ox}$ associated with lipids comes as high as making up the difference between BD simulations with the ChP bilayer and that with the control in their respective fractions of $C2_{ox}$ associated with bc_1 (Fig. S15). These observations suggest that, when the attraction between cyt. c_2 and bc_1 is long-rang, as in a low salt environment, the presence of anionic lipids is unnecessary and distracts the associations of the two proteins. However, anionic lipids have their own functional roles in the chromatophore,[27–29] as in other bioenergetic membranes.[29,70] Removals of anionic lipids for the potentially over-fitting cyt. c_2 - bc_1 association at low salinity will disrupt the overall function of the chromatophore.

4 Conclusion

Anionic lipids are a common feature in all bioenergetic membranes.[71] The present study establishes a diffusion model for cyt. c_2 in the chromatophore, highlighting the influence of anionic lipids on the efficiency of interaction between the redox partners, cyt. c_2 and bc_1, which in turn determines the rate of electron transfer in the whole photosynthetic activity of the organelle.

Our model clearly shows that anionic lipids confine the diffusion of cyt. c_2 to the surface of the membrane, thereby increasing the probability of finding the protein close to the membrane. The resulting localization of cyt. c_2 to the vicinity of the lipid bilayer enhances its likelihood to locate and bind to bc_1, which is an integral protein embedded in the membrane. As a result, despite what might be expected from the potential competition of the lipids with the redox partner for cyt. c_2, the level of association between cyt. c_2 and bc_1 is found to be promoted in the presence of anionic lipids.

This phenomenon, which is observed for both redox forms of cyt. c_2, does not alter the redox-dependence of cyt. c_2 - bc_1 association. Our results suggest that the association of cyt. c_2 to either bc_1 or lipids is also redox-dependent, with the oxidized form of cyt. c_2 exhibiting a stronger binding probability to both bc_1 and lipids. The observed dependence may be attributed to structural differences between the two redox forms of cyt. c_2, which dictate the likelihood for cyt. c_2 - bc_1 association when the protein comes close to bc_1. Preferred association of bc_1 with oxidized cyt. c_2 (compared to reduced cyt. c_2), which is maintained in the presence of anionic lipids, is aligned with the physiological direction of electron transfer mediated by cyt. c_2.

The contribution of anionic lipids to the electron transport process is, however, susceptible to changes in the electrostatic environment, e.g., to the system's salinity. At high salinity (0.4M), the effect of lipids is largely diminished due to screening effects of the salt on cyt. c_2, bc_1, and anionic lipids. Similarly, at very low salinity (0.02M), the enhancement effect of anionic lipids on cyt. c_2 - bc_1 association seems to be largely attenuated. Therefore, for anionic lipids to promote the electron transport process, there seems to be a need for a particular balance between the density of the lipids and the salinity of the environment, and any deviation from this balance can reduce the effect.

Based on the high structural similarity between cyt. c_2/bc_1 and their counterparts in mitochondrial and other bioenergetic membranes, these observations reported here can be

applied to other redox proteins in which electron transfer is mediated by the shuttling of a protein between two integral proteins embedded in an anionic-lipid-rich membrane.

Supplementary Material

Refer to Web version on PubMed Central for supplementary material.

Acknowledgement

This work was supported by the National Institute of General Medical Sciences, Center for Macromolecular Modeling & Bioinformatics, of the National Institutes of Health under award number P41-GM104601. The content is solely the responsibility of the authors and does not necessarily represent the official views of the National Institutes of Health. This research used computational resources at the Oak Ridge Leadership Computing Facility at the Oak Ridge National Laboratory, which is supported by the Office of Science of the U.S. Department of Energy under Contract No. DE-AC05-00OR22725. Additional computational resources were provided by the Blue Waters sustained-petascale computing project, which is supported by the National Science Foundation (awards OCI-0725070 and ACI-1238993) at the State of Illinois, and as of December 2019, the National Geospatial-Intelligence Agency. Blue Waters is a joint effort of the University of Illinois at Urbana-Champaign and its National Center for Supercomputing Applications.

References

(1). Madigan M In The purple phototrophic bacteria; Hunter CN, Daldal F, Thurnauer MC, and Beatty JT, Eds.; Advances in photosynthesis and respiration; Springer, 2008; Vol. 28; pp 1–15.

(2). Cartron ML, Olsen JD, Sener M, Jackson PJ, Brindley AA, Qian P, Dickman MJ, Leggett GJ, Schulten K, and Hunter CN (2014) Integration of energy and electron transfer processes in the photosynthetic membrane of Rhodobacter sphaeroides. Biochimica et Biophysica Acta (BBA) - Bioenergetics 1837, 1769–1780. [PubMed: 24530865]

(3). Sener M, Strümpfer J, Singharoy A, Hunter CN, and Schulten K (2016) Overall energÿ conversion efficiency of a photosynthetic vesicle. eLife 5, e09541. [PubMed: 27564854]

(4). Ritz T, Park S, and Schulten K (2001) Kinetics of excitation migration and trapping in the photosynthetic unit of purple bacteria. J. Phys. Chem. B 105, 8259–8267.

(5). Okamura M, Paddock M, Graige M, and Feher G (2000) Proton and electron transfer in bacterial reaction centers. Biochimica et Biophysica Acta (BBA) - Bioenergetics 1458, 148–163. [PubMed: 10812030]

(6). Scheuring S, and Sturgis JN (2006) Dynamics and diffusion in photosynthetic membranes from Rhodospirillum photometricum. Biophysical Journal 91, 3707–3717. [PubMed: 16950840]

(7). Hauβ T, Dante S, Haines TH, and Dencher NA (2005) Localization of coenzyme Q10 in the center of a deuterated lipid membrane by neutron diffraction. Biochimica et Biophysica Acta (BBA) - Bioenergetics 1710, 57–62. [PubMed: 16199002]

(8). Singharoy A, Barragan AM, Thangapandian S, Tajkhorshid E, and Schulten K (2016) Binding Site recognition and docking dynamics of a single electron transport protein: cytochrome c_2. J. Am. Chem. Soc 138, 12077–12089. [PubMed: 27508459]

(9). Boris A Feniouk WJ In The purple phototrophic bacteria; Hunter CN, Daldal F, Thurnauer MC, and Beatty JT, Eds.; Advances in photosynthesis and respiration; Springer, 2008; Vol. 28; pp 475–493.

(10). Kramer DM, Nitschke W, and Cooley JW In The purple phototrophic bacteria; Hunter CN, Daldal F, Thurnauer MC, and Beatty JT, Eds.; Advances in photosynthesis and respiration; Springer, 2009; Vol. 28; pp 451–473.

(11). Geyer T, and Helms V (2006) Reconstruction of a kinetic model of the chromatophore vesicles from Rhodobacter sphaeroides. Biophysical Journal 91, 927–937. [PubMed: 16714340]

(12). Milano F, Agostiano A, Mavelli F, and Trotta M (2003) Kinetics of the quinone binding reaction at the QB site of reaction centers from the purple bacteria *Rhodobacter sphaeroides* reconstituted in liposomes. European Journal of Biochemistry 270, 4595–4605. [PubMed: 14622246]

(13). Swainsbury DJ, Proctor MS, Hitchcock A, Cartron ML, Qian P, Martin EC, Jackson PJ, Madsen J, Armes SP, and Hunter CN (2018) Probing the local lipid environment of the *Rhodobacter sphaeroides* cytochrome bc_1 and *Synechocystis* sp. PCC 6803 cytochrome b_6f complexes with styrene maleic acid. Biochimica et Biophysica Acta (BBA) - Bioenergetics 1859, 215–225. [PubMed: 29291373]

(14). Singharoy A et al. (2019) Atoms to phenotypes: molecular design principles of cellular energy metabolism. Cell 179, 1098–1111.e23. [PubMed: 31730852]

(15). Singharoy A, Chipot C, Moradi M, and Schulten K (2017) Chemomechanical coupling in hexameric protein-protein interfaces harnesses energy within V-type ATPases. J. Am. Chem. Soc 139, 293–310. [PubMed: 27936329]

(16). Sarewicz M, Pietras R, Froncisz W, and Osyczka A (2011) Reorientation of cytochrome c_2 upon interaction with oppositely charged macromolecules probed by SR EPR: implications for the role of dipole moment to facilitate collisions in proper configuration for electron transfer. Metallomics 3, 404–409. [PubMed: 21431229]

(17). Tiede DM, Vashishta A-C, and Gunner MR (1993) Electron-transfer kinetics and electrostatic properties of the *Rhodobacter sphaeroides* reaction center and soluble ccytochromes. Biochemistry 32, 4515–4531. [PubMed: 8387335]

(18). Zhang X, Hiser C, Tamot B, Benning C, Reid GE, and Ferguson-Miller SM (2011) Combined genetic and metabolic manipulation of lipids in *Rhodobacter sphaeroides* reveals non-phospholipid substitutions in fully active cytochrome *c* oxidase. Biochemistry 50, 3891–3902. [PubMed: 21476580]

(19). Russell NJ, and Harwood JL (1979) Changes in the acyl lipid composition of photosynthetic bacteria grown under photosynthetic and non-photosynthetic conditions. Biochemical Journal 181, 339–345.

(20). Yu SP, and Choi DW (2000) Ions, cell volume, and apoptosis. Proceedings of the National Academy of Sciences 97, 9360–9362.

(21). Alvarez-Paggi D, Hannibal L, Castro MA, Oviedo-Rouco S, Demicheli V, Tórtora V, Tomasina F, Radi R, and Murgida DH (2017) Multifunctional cytochrome *c*: learning new tricks from an old dog. Chemical Reviews 117, 14014–14014. [PubMed: 29192778]

(22). Díaz-Quintana A, Pérez-Mejías G, Guerra-Castellano A, De la Rosa MA, and Díaz-Moreno I (2020) Wheel and deal in the mitochondrial inner membranes: the tale of cytochrome *c* and cardiolipin. Oxidative Medicine and Cellular Longevity 2020, 6813405. [PubMed: 32377304]

(23). Vasilev C, Mayneord GE, Brindley AA, Johnson MP, and Hunter CN (2019) Dissecting the cytochrome c_2-reaction centre interaction in bacterial photosynthesis using single molecule force spectroscopy. Biochemical Journal 476, 2173–2190.

(24). Lange C, and Hunte C (2002) Crystal structure of the yeast cytochrome bc_1 complex with its bound substrate cytochrome *c*. Proceedings of the National Academy of Sciences 99, 2800–2805.

(25). Hunte C, Solmaz S, and Lange C (2002) Electron transfer between yeast cytochrome bc1 complex and cytochrome c: a structural analysis. Biochimica et Biophysica Acta (BBA) - Bioenergetics 1555, 21–28. [PubMed: 12206886]

(26). Pöyry S, Cramariuc O, Postila PA, Kaszuba K, Sarewicz M, Osyczka A, Vattulainen I, and Róg T (2013) Atomistic simulations indicate cardiolipin to have an integral role in the structure of the cytochrome bc1 complex. Biochimica et Biophysica Acta (BBA) - Bioenergetics 1827, 769–778. [PubMed: 23529178]

(27). Leo VD, Catucci L, Ventrella A, Milano F, Agostiano A, and Corcelli A (2009) Cardiolipin increases in chromatophores isolated from *Rhodobacter sphaeroides* after osmotic stress: structural and functional roles. Journal of Lipid Research 50, 256–264. [PubMed: 18716316]

(28). Birrell GB, Sistrom WR, and Griffith OH (1978) Lipid-protein associations in chromatophores from the photosynthetic bacterium *Rhodopseudomonas sphaeroides*. Biochemistry 17, 3768–3773. [PubMed: 212104]

(29). Lucia C, Vincenzo DL, Francesco M, Livia G, Rita V, Agostiano A, and Angela C (2012) Oxidoreductase activity of chromatophores and purified cytochrome bc_1 complex from *Rhodobacter sphaeroides*: a possible role of cardiolipin. Journal of Bioenergetics and Biomembranes 44, 487–493. [PubMed: 22733014]

(30). McGuffee SR, and Elcock AH (2010) Diffusion, crowding & protein stability in a dynamic molecular model of the bacterial cytoplasm. PLOS Computational Biology 6, 1–18.

(31). Northrup SH, Boles JO, and Reynolds JCL (1988) Brownian dynamics of cytochrome *c* and cytochrome *c* peroxidase association. Science 241, 67–70. [PubMed: 2838904]

(32). Gross EL, and Pearson DC (2003) Brownian dynamics simulations of the interaction of chlamydomonas cytochrome *f* with plastocyanin and cytochrome c_6. Biophysical Journal 85, 2055–2068. [PubMed: 12944318]

(33). Nakagawa S, Kurniawan I, Kodama K, Arwansyah MS, Kawaguchi K, and Nagao H (2018) Theoretical study on interaction of cytochrome *f* and plastocyanin complex by a simple coarse-grained model with molecular crowding effect. Molecular Physics 116, 666–677.

(34). Pérez-Mejías G, Guerra-Castellano A, Díaz-Quintana A, la Rosa MAD, and Díaz-Moreno I (2019) Cytochrome *c*: surfing off of the mitochondrial membrane on the tops of complexes III and IV. Computational and Structural Biotechnology Journal 17, 654–660. [PubMed: 31193759]

(35). Esser L, Elberry M, Zhou F, Yu C-A, Yu L, and Xia D (2008) Inhibitor-complexed structures of the cytochrome bc_1 from the photosynthetic bacterium *Rhodobacter sphaeroides*. Journal of Biological Chemistry 283, 2846–2847.

(36). Humphrey W, Dalke A, and Schulten K (1996) VMD – Visual Molecular Dynamics. J Mol Graph 14, 33–38. [PubMed: 8744570]

(37). Huang J, Rauscher S, Nawrocki G, Ran T, Feig M, de Groot BL, Grubmuller H, and MacKerell AD Jr (2017) CHARMM36m: an improved force field for folded and intrinsically disordered proteins. Nature Methods 14, 71–73. [PubMed: 27819658]

(38). Autenrieth F, Tajkhorshid E, Baudry J, and Luthey-Schulten Z (2004) Classical force field parameters for the heme prosthetic group of cytochrome *c*. Journal of Computational Chemistry 25, 1613–1622. [PubMed: 15264255]

(39). Lomize MA, Pogozheva ID, Joo H, Mosberg HI, and Lomize AL (2011) OPM database and PPM web server: resources for positioning of proteins in membranes. Nucleic Acids Research 40, D370–D376. [PubMed: 21890895]

(40). Jo S, Kim T, and Im W (2007) Automated builder and database of protein/membrane complexes for molecular dynamics simulations. PLOS ONE 2, 1–9.

(41). Jo S, Kim T, Iyer VG, and Im W (2008) CHARMM-GUI: A Web-Based Graphical User Interface for CHARMM. Journal of Computational Chemistry 29, 1859–1865. [PubMed: 18351591]

(42). Jo S, Lim JB, Klauda JB, and Im W (2009) CHARMM-GUI membrane builder for mixed bilayers and its application to yeast membranes. Biophysical Journal 97, 50–58. [PubMed: 19580743]

(43). Wu E, Cheng X, Jo S, Rui H, Song K, Dávila-Contreras E, Qi Y, Lee J, Monje-Galvan V, Venable R, Klauda J, and Im W (2014) CHARMM-GUI Membrane Builder toward realistic biological membrane simulations. Journal of Computational Chemistry 35, 1997–2004. [PubMed: 25130509]

(44). Kates M, Syz J-Y, Gosser D, and Haines TH (1993) pH-dissociation characteristics of cardiolipin and its 2'-deoxy analogue. Lipids 28, 887–882.

(45). Hielscher R, Wenz T, Hunte C, and Hellwig P (2009) Monitoring the redox and protonation dependent contributions of cardiolipin in electrochemically induced FTIR difference spectra of the cytochrome bc_1 complex from yeast. Biochimica et Biophysica Acta (BBA) - Bioenergetics 1787, 617–625. [PubMed: 19413949]

(46). Olofsson G, and Sparr E (2013) Ionization constants pK_a of cardiolipin. PLOS ONE 8, 1–6.

(47). Sathappa M, and Alder NN (2016) The ionization properties of cardiolipin and its variants in model bilayers. Biochimica et Biophysica Acta (BBA) - Biomembranes 1858, 1362–1372. [PubMed: 26965987]

(48). Axelrod HL, Abresch EC, Okamura MY, Yeh AP, Ress DC, and Feher G (2002) X-ray structure determination of the cytochrome c_2: reaction center electron transfer complex from *Rhodobacter sphaeroides*. Journal of Molecular Biology 319, 501–515. [PubMed: 12051924]

(49). Phillips JC, Braun R, Wang W, Gumbart J, Tajkhorshid E, Villa E, Chipot C, Skeel RD, Kale L, and Schulten K (2005) Scalable molecular dynamics with NAMD. Journal of Computational Chemistry 26, 1781–1802. [PubMed: 16222654]

(50). Phillips JC et al. (2020) Scalable molecular dynamics on CPU and GPU architectures with NAMD. The Journal of Chemical Physics 153, 044130. [PubMed: 32752662]

(51). Ortega A, Amorós D, and de la Torre JG (2011) Prediction of hydrodynamic and other solution properties of rigid proteins from atomic- and residue-level models. Biophysical Journal 101, 892–898. [PubMed: 21843480]

(52). Berkhin P In Grouping multidimensional data: recent advances in clustering; Kogan J, Nicholas C, and Teboulle M, Eds.; Springer, 2006; pp 25–71.

(53). Ahmad A, and Dey L (2007) A *k*-mean clustering algorithm for mixed numeric and categorical data. Data & Knowledge Engineering 63, 503–527.

(54). Baker NA, Sept D, Joseph S, Holst MJ, and McCammon JA (2001) Electrostatics of nanosystems: application to microtubules and the ribosome. Proceedings of the National Academy of Sciences 98, 10037–10041.

(55). Jurrus E et al. (2018) Improvements to the APBS biomolecular solvation software suite. Protein Science 27, 112–128. [PubMed: 28836357]

(56). Cohen J, Arkhipov A, Braun R, and Schulten K (2006) Imaging the migration pathways for O2, CO, NO, and Xe inside myoglobin. Biophysical Journal 91, 1844–1857. [PubMed: 16751246]

(57). Comer J, and Aksimentiev A (2012) Predicting the DNA sequence dependence of nanopore ion current using atomic-resolution Brownian dynamics. J. Phys. Chem C 116, 3376–3393.

(58). Venturoli G, Gabellini N, Oesterhelt D, and Melandri BA (1990) Kinetics of photosynthetic electron transfer in artificial vesicles reconstituted with purified complexes from *Rhodobacter capsulatus*. European Journal of Biochemistry 189, 95–103. [PubMed: 2158893]

(59). Wennerström H, Vallina Estrada E, Danielsson J, and Oliveberg M (2020) Colloidal stability of the living cell. Proceedings of the National Academy of Sciences 117, 10113–10121.

(60). Li M, Sun W, Tyurin VA, DeLucia M, Ahn J, Kagan VE, and van der Wel PC (2021) Activation of cytochrome *c* peroxidase function through coordinated foldon loop dynamics upon interaction with anionic lipids. Journal of Molecular Biology 433, 167057. [PubMed: 34033821]

(61). McAuley KE, Fyfe PK, Ridge JP, Isaacs NW, Cogdell RJ, and Jones MR (1999) Structural details of an interaction between cardiolipin and an integral membrane protein. Proceedings of the National Academy of Sciences 96, 14706–14711.

(62). Schlame M, and Ren M (2009) The role of cardiolipin in the structural organization of mitochondrial membranes. Biochimica et Biophysica Acta (BBA) - Biomembranes 1788, 2080–2083. [PubMed: 19413994]

(63). Mao X, Yao S, Yi Q, Xu Z-M, and Cang X (2021) Function-related asymmetry of the specific cardiolipin binding sites on the mitochondrial ADP/ATP carrier. Biochimica et Biophysica Acta (BBA) - Biomembranes 1863, 183466. [PubMed: 32871114]

(64). Moré JJ, and Sorensen D (1983) Computing a trust region step. SIAM Journal on Scientific and Statistical Computing 3, 553–572.

(65). Imai M, Saio T, Kumeta H, Uchida T, Inagaki F, and Ishimori K (2016) Investigation of the redox-dependent modulation of structure and dynamics in human cytochrome *c*. Biochemical and Biophysical Research Communications 469, 978–984. [PubMed: 26718409]

(66). Banci L, Bertini I, Bren KL, Gray HB, Sompornpisut P, and Turano P (1997) Solution structure of oxidized *Saccharomyces cerevisiae* iso-1-cytochrome *c*,. Biochemistry 36, 8992–9001. [PubMed: 9220987]

(67). Baxter SM, and Fetrow JS (1999) Hydrogen exchange behavior of [U-^{15}N]-labeled oxidized and reduced iso-1-cytochrome *c*. Biochemistry 38, 4493–4503. [PubMed: 10194371]

(68). Fetrow JS, and Baxter SM (1999) Assignment of ^{15}N chemical shifts and ^{15}N relaxation measurements for oxidized and reduced iso-1-cytochrome *c*. Biochemistry 38, 4480–4492. [PubMed: 10194370]

(69). Volkov AN, Vanwetswinkel S, Van de Water K, and van Nuland NAJ (2012) Redox-dependent conformational changes in eukaryotic cytochromes revealed by paramagnetic NMR spectroscopy. Journal of Biomolecular NMR 52, 245–256. [PubMed: 22318343]

(70). Lange C, Nett JH, Trumpower BL, and Hunte C (2001) Specific roles of protein-phospholipid interactions in the yeast cytochrome bc_1 complex structure. The EMBO Journal 20, 6591–6600. [PubMed: 11726495]

(71). Horvath SE, and Daum G (2013) Lipids of mitochondria. Progress in Lipid Research 52, 590–614. [PubMed: 24007978]

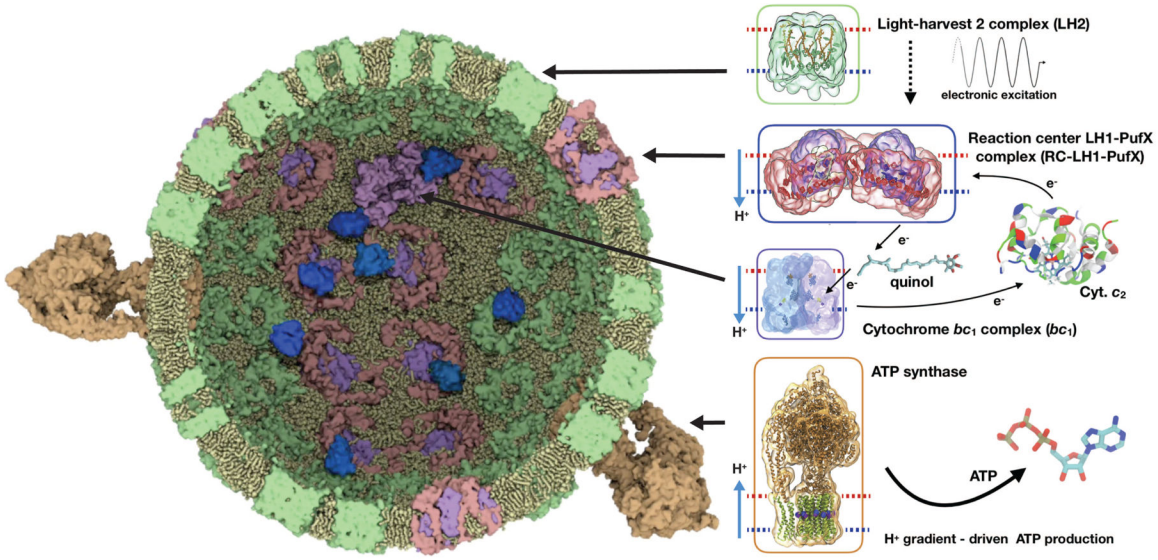

Figure 1: The role of cyt. c_2 shuttling in the photon-induced ATP production in the chromatophore.

Cross-sectional view of a molecular model[2,3,14] for the chromatophore in the purple bacteria is shown on the left, with bc_1 (PDB: 2QJY), LH2 (PDB: 1NKZ), and ATP synthase (PDB: 3VR2)[15] colored in purple, light green, and light brown, respectively. For the RC-LH1-PufX (PDB: 6ET5) sites, where RC and LH1 form complexes, RC are colored in light purple and LH1 in magenta. Cyt. c_2 (PDB: 1L9B) proteins, colored in blue, are mobile and shuttle inside the chromatophore. On the right, processes of light energy transfer and electron transport are summarized. Proton (H^+) translocation across the chromatophore membrane is indicated by blue arrows, with the side of the membrane facing the exterior (interior) of the chromatophore represented by a red (blue), dashed line. Reprinted with permission from ref.[14] Copyright 2019 CELL Press.

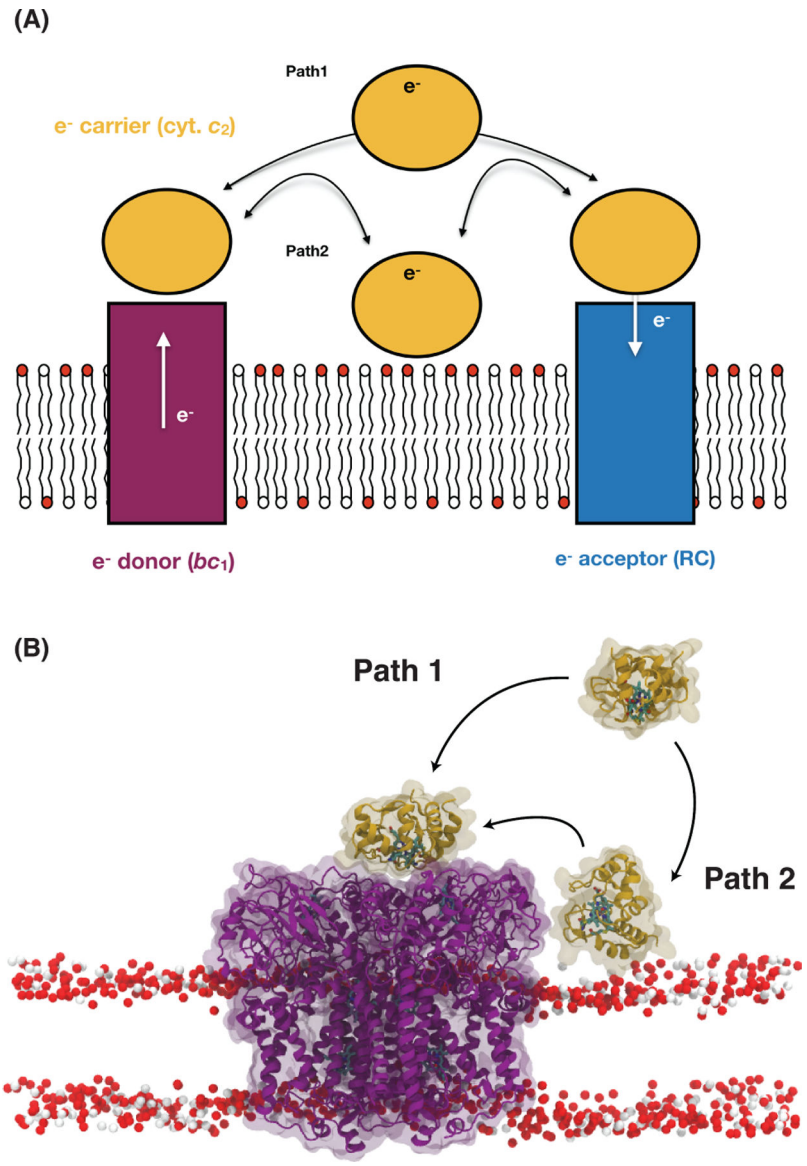

Figure 2: Interplay of transmembrane redox proteins, soluble electron-shuttling proteins, and lipids in bioenergetic membranes.

(**A**) Respiratory and photosynthetic membranes employ soluble, shuttling proteins (yellow) to mediate electron (e^-) transport between transmembrane redox protein complexes (purple and blue). During this process, the shuttling protein diffuses between the electron-donor (magenta) and -acceptor (blue) proteins frequently. The lipid phase of the membrane, which is often rich in negative charges (red circles) in bioenergetic membranes,[34] can both confine the diffusion of the soluble protein to the surface of the membrane and/or directly affect its mobility. Diffusing without interaction with membrane lipids (largely diffusing in bulk solution) is denoted as Path 1. In the case of diffusion on the surface of the membrane while interacting with anionic lipids (Path 2), the soluble protein remains close to the membrane surface, and its motion can be described as a 2D diffusion. Surface-bounded diffusion has been hypothesized to exist as a result of the ubiquitous presence of negative charges in bioenergetic membranes. In purple bacterial chromatophore, cyt. c_2, the soluble protein,

shuttles between bc_1, the e^- donor, and RC, the e^- receptor. (**B**) Molecular representations of cyt. c_2 (yellow) and bc_1 (purple), and the two types of cyt. c_2 diffusion (Paths 1 and 2) to bind to bc_1. The phosphorus atoms of lipid molecules in the membrane are shown as red spheres for anionic lipids and as white spheres for other lipids.

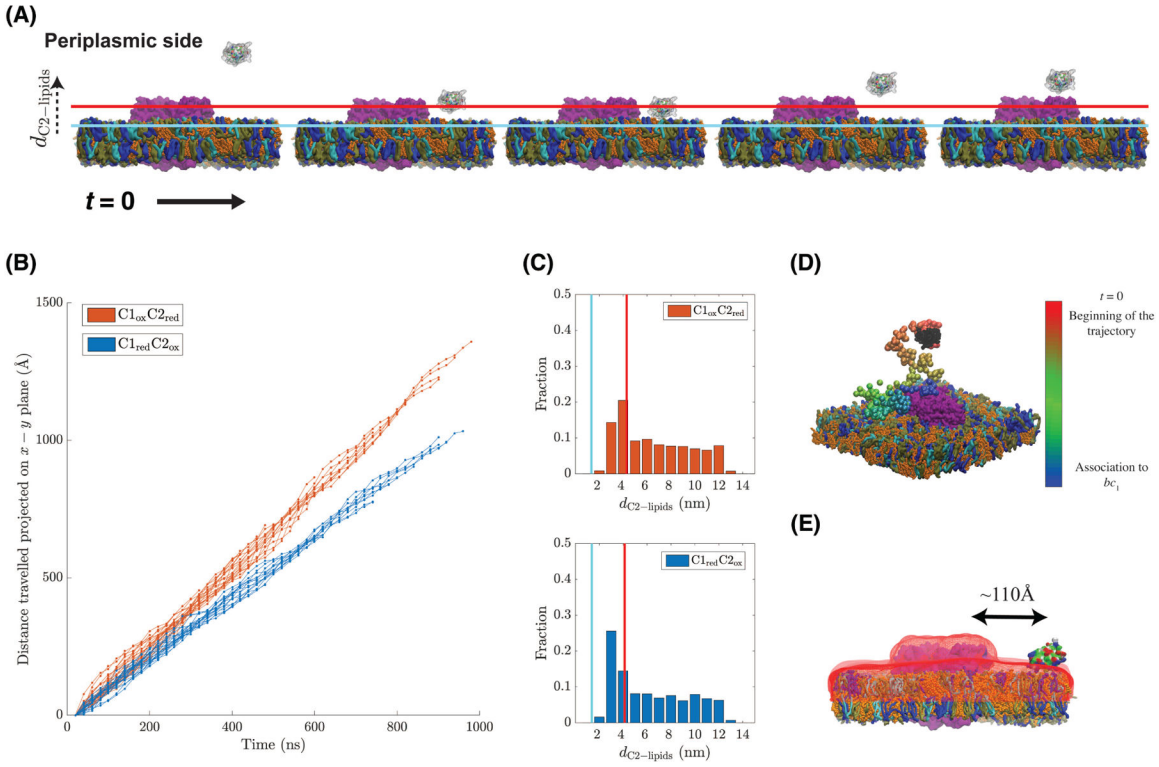

Figure 3: Lipid-Mediated Association of cyt. c_2 to bc_1 ($LMA_{C2\rightarrow C1}$).

(**A**) Snapshots depicting an example of $LMA_{C2\rightarrow C1}$. The process involves initial association of cyt. c_2 to the lipid bilayer, followed by its hopping onto bc_1. These different stages are shown chronologically from the left to the right. The approximate surface of the lipid bilayer and bc_1 are marked by cyan and red lines, respectively. The region between these lines is considered as the vicinity of the lipid bilayer (Sec.S1.5). The quantity, $d_{C2-lipids}$ (Sec. S1.5), denotes the separation of the center of mass (COM) of cyt. c_2 from the membrane's phosphorus plane on the periplasmic side. bc_1 is shown in purple; the PC, PE, PG, and CL lipids are shown in blue, cyan, dark green, and orange, respectively. Same coloring scheme used in (D) and (E). (**B**) Distance travelled by cyt. c_2 after its first lipid association during $LMA_{C2\rightarrow C1}$, calculated only in the *xy* plane (i.e., along the membrane surface). For each $LMA_{C2\rightarrow C1}$ event, the measurement starts from first binding of cyt. c_2 to the lipid bilayer and ends when it associated with bc_1. (**C**) Distribution of $d_{C2-lipids}$ distances defined in (A), for all cyt. c_2 cases involved in $LMA_{C2\rightarrow C1}$. $d_{C2-lipids}$ was measured from the time cyt. c_2 associates with the lipids until it binds bc_1. The red and cyan lines are defined in (A). (**D**) A representative trajectory of $LMA_{C2\rightarrow C1}$. The COM of cyt. c_2 at each time point is drawn as a sphere, with its color indicating the time (shown in the color bar). A surface representation for cyt. c_2, instead of just its COM, at $t = 0$ is shown in black. (**E**) An example of a lipid-associated cyt. c_2 located ~110 Å from bc_1, a distance that represents the average cyt. c_2-bc_1 separation at the first encounter of cyt. c_2 with lipids during an $LMA_{C2\rightarrow C1}$ event. The electrostatic potential (red) of the bc_1-embedded membrane is shown by its contour surface at $-0.5k_BT$.

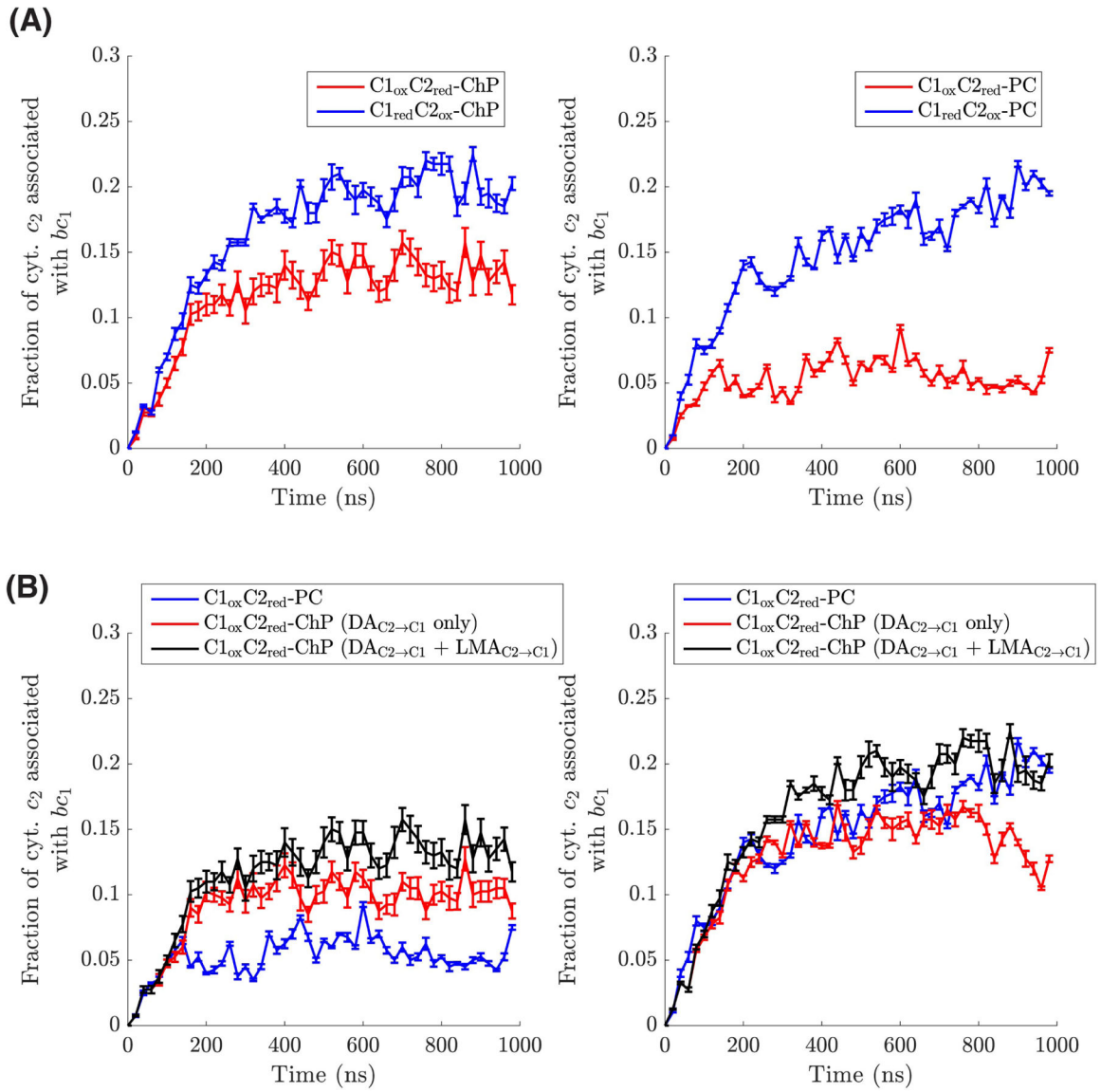

Figure 4: Impacts of anionic lipids on cyt. c_2 - bc_2 associations

(A)&(B) Time evolution of the fraction of cyt. c_2 associated with bc_1. The legend, "$C1_xC2_Y$-Z", indicates the redox state of bc_1 (x), the redox state of cyt. c_2 (Y), and the type of lipid bilayer employed in the specific set of BD simulations (Sec. 2.5 of Methods). An oxidized state is denoted as "ox", and a reduced state is denoted as "red". The control bilayer and the chromatophore-like bilayer are denoted as "PC" and "ChP", respectively. In (B), the time evolution for BD simulations employing the ChP bilayer are shown as 2 types of time series, one with and another without contributions from $LMA_{C2\rightarrow C1}$ (Sec.3.1 of Results and Discussions). The ones without contributions from $LMA_{C2\rightarrow C1}$ only consist of contributions from which cyt. c_2 diffuse to and associate with bc_1 completely in the bulk solution without any lipid association. This type of associations is here coined as Direct Association of cyt. c_2 to bc_1 ($DA_{C2\rightarrow C1}$). Our data for $C2_{red}$ reveals a straight forward enhancement to cyt. c_2 - bc_1 associations upon the presence of an electro-negative membrane (CL); where as a more complicated condition is found for $C2_{ox}$. This complication is discussed in the main text.

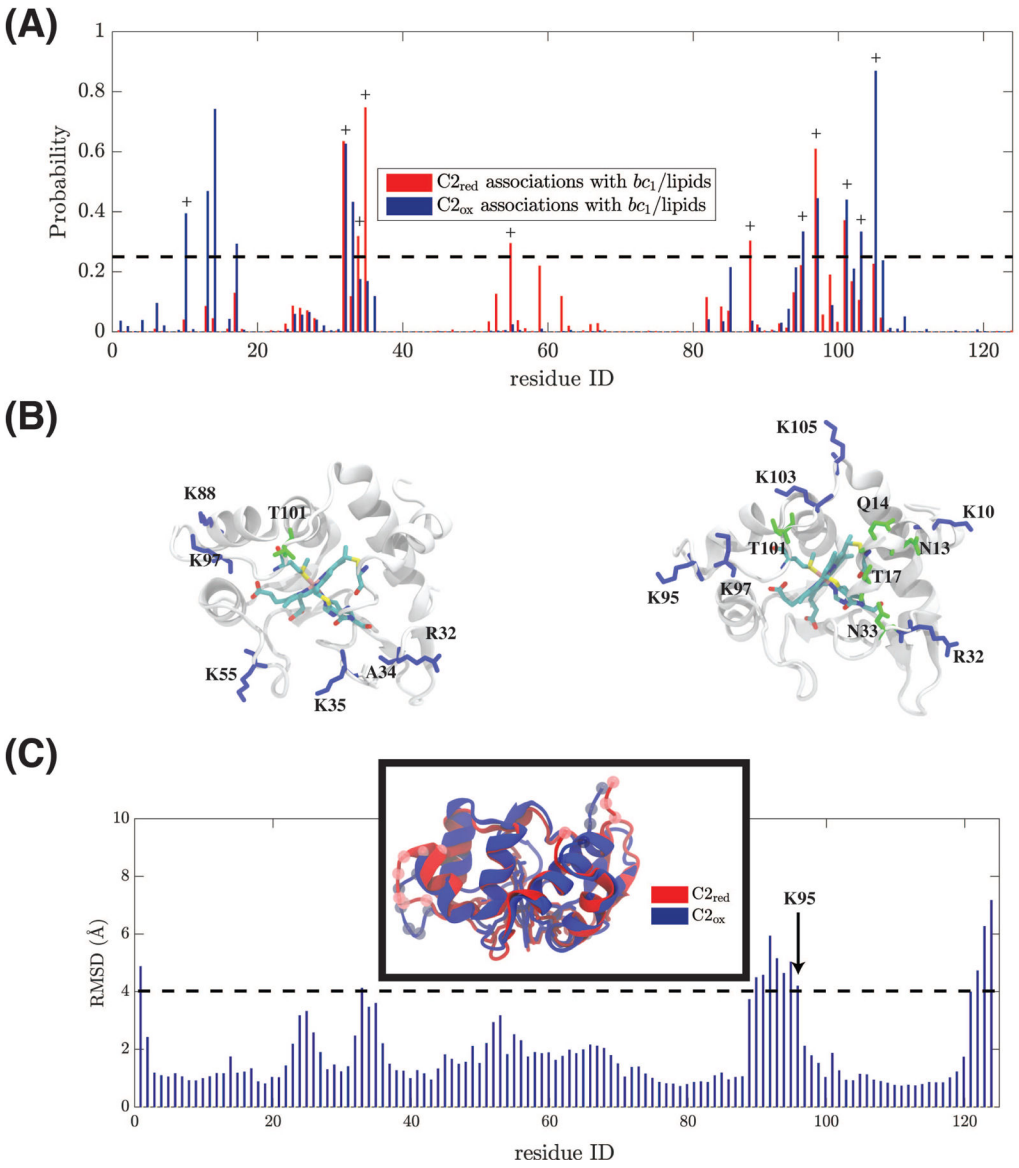

Figure 5: Effect of the redox state of cyt. c_2 on its interactions with bc_1 and lipids.

(**A**) Probabilities for individual residues of cyt. c_2 to make contacts with an association partner for $C2_{red}$ and $C2_{ox}$ (Sec. S1.3). The probability threshold (>0.25) used to classify hotspot residues is indicated by a dashed line. Basic hotspot residues are marked by a '+' sign. No acidic hotspot residues were observed. (**B**) Hotspot residues for $C2_{red}$ (left) and $C2_{ox}$ (right) are shown in licorice representations and labeled. Basic residues are in blue, polar ones in green, and A34 from $C2_{red}$ (non-polar) is in white. (**C**) Residue-based root mean squared deviations (RMSDs) between $C2_{red}$ and $C2_{ox}$, averaged over the MD simulations (Sec. 2.1). The Cα atoms of residues with RMSDs higher than 4 Å(dashed line) are shown as glassy spheres in the molecular image. The inset displays an overlay of $C2_{ox}$ (blue) and $C2_{red}$ (red) structures, obtained from the last frame of MD simulations, indicating high structural similarity between the two redox forms.

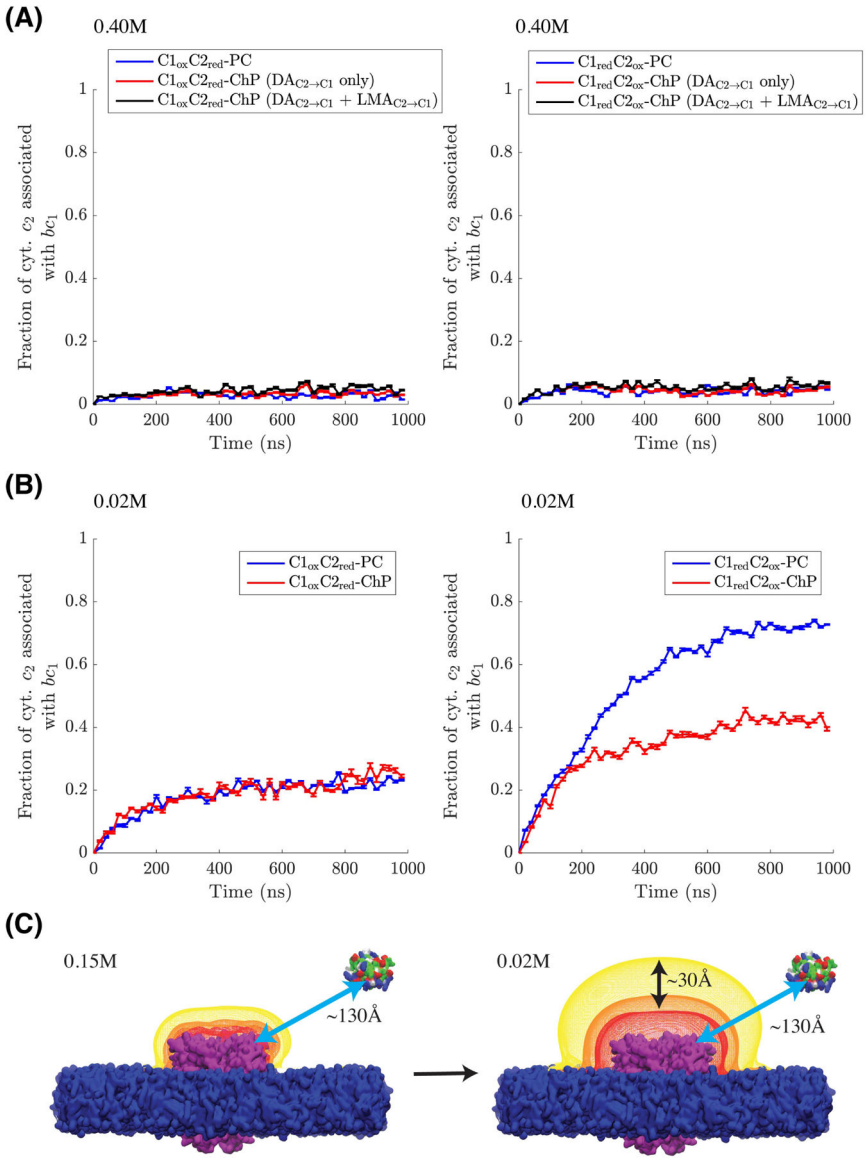

Figure 6: Impact of salinity on cyt. c_2-bc_1 association.

(A) and (B) Time evolution of the fraction of cyt. c_2 associated with bc_1 for BD simulations at 0.40M (A) and 0.02M (B) salinity. (**C**) Change in the electrostatic potential of bc_1 upon reduction of salinity from 0.15M to 0.02M. The potential shown is derived from the control membranes to focus the comparison only on the electrostatic potential of bc_1. Cross sectional views of contour surfaces corresponding to the potentials at −1 $k_B T$, −0.5 $k_B T$, and −0.1 $k_B T$ are shown in red, orange, and yellow, respectively. The outward expansion of the yellow contour surface upon the decreased salinity is around 30 Å, and is indicated by a black arrow. For cyt. c_2 associating to bc_1 through $LMA_{C2\to C1}$, their mean separation from bc_1 at the beginning of respective BD simulations is 130 Å (Fig. S11). This separation is indicated by a cyan arrow in each sub-figure.

Table 1:

Recognition probabilities $\left(p_A^{\mathrm{C2_{red}}}, p_A^{\mathrm{C2_{ox}}}\right)$ and residence probabilities $\left(p_{A\to A}^{\mathrm{C2_{red}}}, p_{A\to A}^{\mathrm{C2_{ox}}}\right)$ for $\mathbf{C2_{red}}$ and $\mathbf{C2_{ox}}$ with *A*.

The association partner, *A*, is chosen from reducedbc_1 ($C1_{red}$), oxidizedbc_1 ($C1_{ox}$), and lipids of the chromatophore-like bilayer. These probabilites are shown here in the unit of percentage (%), where 1% = 0.01. These probabilities show that, the likelihood, and hence the ability, for cyt.c_2 to recognize an association partner when it is in the bulk solution is only marginally affected by the protein redox state; whereas the protein ability to stay associated with an association partner is appreciably controlled by the protein redox state. Determinations of these probabilities are given in Sec.S1.4. "*NA*" stands for not applicable.

	$p_A^{\mathrm{C2_{red}}}$	$p_A^{\mathrm{C2_{ox}}}$	$p_{A\to A}^{\mathrm{C2_{red}}}$	$p_{A\to A}^{\mathrm{C2_{ox}}}$
$A = C1_{red}$	*NA*	5% ± 0.3%	*NA*	40% ± 4%
$A = C1_{ox}$	4% ± 0.2%	*NA*	33% ± 2%	*NA*
A = lipids	5% ± 0.1%	6% ± 0.2%	34% ± 1%	43% ± 2%